Hindawi Publishing Corporation
EURASIP Journal on Advances in Signal Processing
Volume 2008, Article ID 916865, 14 pages
doi:10.1155/2008/916865

Research Article

Crosstalk Channel Estimation via Standardized Two-Port Measurements

Fredrik Lindqvist,[1] Neiva Lindqvist,[2] Boris Dortschy,[3] Per Ödling,[1] Per Ola Börjesson,[1] Klas Ericson,[3] and Evaldo Pelaes[2]

[1] *Department of Electrical and Information Technology, Lund University, 221 00 Lund, Sweden*
[2] *Signal Processing Laboratory (LaPS), Federal University of Para, 66075-110 Belem, PA, Brazil*
[3] *Ericsson Research, Broadband Technologies, Ericsson AB, 16480 Stockholm, Sweden*

Correspondence should be addressed to Fredrik Lindqvist, fredrik.lindqvist@eit.lth.se

Received 21 September 2008; Accepted 19 December 2008

Recommended by Jonathon Chambers

The emerging multiuser transmission techniques for enabling higher data rates in the copper-access network relies upon accurate knowledge of the twisted-pair cables. In particular, the square-magnitude of the crosstalk channels between the transmission lines are of interest for crosstalk-mitigation techniques. Acquiring such information normally requires dedicated apparatus since crosstalk-channel measurement is not included in the current digital subscriber line (DSL) standards. We address this problem by presenting a standard-compliant estimator for the square-magnitude of the frequency-dependent crosstalk channels that uses only functionality existing in today's standards. The proposed estimator is evaluated by laboratory experiments with standard-compliant DSL modems and real copper access network cables. The estimation results are compared with both reference measurements and with a widely used crosstalk model. The results indicate that the proposed estimator obtains an estimate of the square-magnitude of the crosstalk channels with a mean deviation from the reference measurement less than 3 dB for most frequencies.

1. INTRODUCTION

One of the main impairments for high-speed digital subscriber line (DSL) systems is the destructive crosstalk from neighboring DSL systems. The interfering crosstalk occurs when neighboring systems transmit in the same spectrum due to the inherent electromagnetic coupling between the twisted-pair cables colocated in the same copper access binder (bundle). Both near-end crosstalk (NEXT) and far-end crosstalk (FEXT) occur, where NEXT(FEXT) refers to the crosstalk caused by the transmitter(s) on the same (opposite) side of the line. The NEXT and FEXT interferences in a copper access binder are illustrated in Figure 1. In order to achieve higher data-rates in the access network, many new proposed multiuser transmission techniques utilize accurate knowledge of the transmission paths in the cable binder.

An important multiuser transmission approach that has received a lot of attention recently is *dynamic spectrum management* (DSM) [1–4]. For DSM aiming at *crosstalk mitigation* [5–11], the power spectral density (PSD) of the individual transmitters is usually optimized in such a way that (e.g., the total data rate (throughput)) is maximized, and/or the total transmitted power is minimized. Most of the spectrum management algorithms have been developed assuming perfect (crosstalk) channel information. Especially the square-magnitude of the FEXT channels (i.e., the attenuation) is assumed known a priori. The NEXT is of less concern for DSM due to the usage of frequency division duplex (FDD) for separation of the upstream and downstream frequency bands, employed by the majority of all ADSL [12, 13] and VDSL [14] connections. It is worth noting that for crosstalk *cancellation* methods, which are not considered in this work, the phase also has to be estimated or assumed known.

One option to create up-to-date information about the transmission lines is to use one-port measurements referred to as single-ended line testing (SELT) [15–20]. From the SELT measurement the line length can be estimated, which,

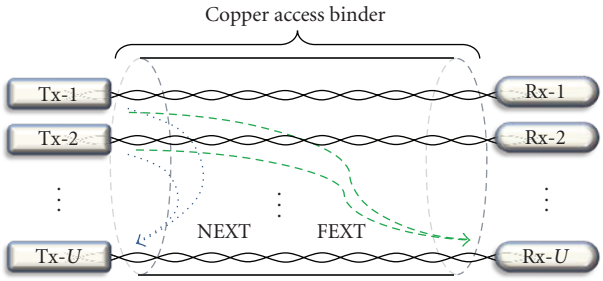

Figure 1: NEXT and FEXT interferences in a copper cable binder for a DSL network with U number of near-end transmitters (Tx) and far-end receivers (Rx).

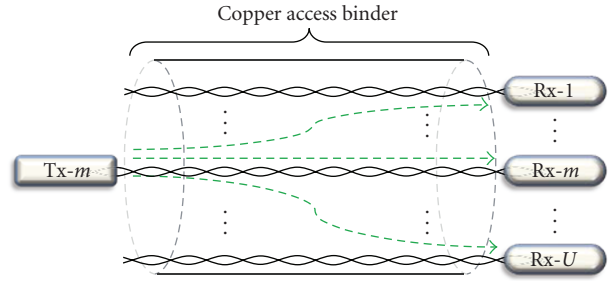

Figure 2: Sequential SIMO transmission with only one active transmitter (Tx) per estimation sequence $m = 1, 2, \ldots, U$. The far-end receivers (Rx) measure the FEXT for each sequence, whereupon the MIMO FEXT channel matrix can be estimated. The MIMO NEXT channel matrix can be estimated in the same way by using Rx:s located at the same side of the binder as Tx.

together with a length-dependent crosstalk model [21, 22], can be used to roughly estimate the square-magnitude of the NEXT/FEXT channel. However, as reported in [23, 24], the frequency-dependent crosstalk channels can vary significantly, and in a stochastic way, between different twisted-pair lines of the same length. This fact was considered in [24] which extends the standardized crosstalk model [21, 22], based on measurements and stochastic analysis, by including phase information and variation of the coupling functions. However, given only the length of the line, the accuracy is still not satisfying.

A general drawback with one-port-based methods, applied to crosstalk channel estimation, is the high attenuation of the crosstalk channel, which becomes a major drawback since the SELT signal has to travel back and forth. In literature, several two-port estimation methods have been considered [25–29]. In [25], an impartial third-party site identifies the crosstalk channels of the binder. Transmitted and received signals from all modems in the binder are collected during a given time span. Initially, a cross-correlation technique is applied to estimate the timing differences between the signals from different providers in the same binder. Thereafter, a least-square method is used to jointly estimate the crosstalk channels and to further improve the timing offsets. In [26], the NEXT crosstalk sources are identified in the frequency domain by finding the maximum correlation with a "basis set" of representative measured crosstalk couplings. However, this method does not apply to FEXT estimation. In [27], a real-time FEXT crosstalk identification is proposed by using the initialization procedure of a newly activated modem and applying a least-square estimator. The authors of [28] derive "blocked state-space models" for multirate xDSL networks and set up the mapping relationship between available input and output data. The least-square principle is further used to identify the crosstalk channels. In [29] an iterative method is described that estimates the FEXT channels based on measured and reported signal-to-noise ratios. The purpose in [29] is to cancel the self-FEXT by precoding, and therefore, both amplitude and phase of the channels are estimated.

This paper describes an estimator for simultaneously obtaining the square-magnitude of the FEXT and NEXT channels of a copper access cable binder. More specifically, the aim is to estimate the multiple-input multiple-output (MIMO) FEXT and NEXT channel matrices. By employing a sequential single-input multiple-output (SIMO) estimation procedure, as illustrated in Figure 2, we provide an accurate estimate of the crosstalk channels which commonly are assumed known a priori by the published DSM crosstalk mitigation techniques. In contrast to [25–28], the proposed estimator requires no hardware or software changes of the DSL modems, and utilizes only measurements available via the existing DSL standards [12–14]. Thus, the estimator provides an immediately available low-cost solution based on standardized signals and protocols. In line with [25], we propose a co-ordinated measurement period during a given time span where the estimation is carried out. Since the square-magnitude of the crosstalk channels does not (normally) vary with time, at least not significantly, the estimation only has to be done once or seldom.

The paper is organized as follows. In Section 2 we introduce the system and signals used by the proposed estimator, followed by the MIMO and the SIMO modeling applied in this work. Based on these transmission models, Section 3 describes the proposed estimator for obtaining the square-magnitude of FEXT and NEXT channels. A practical implementation of the estimator is described in Section 4. The FEXT model used for the evaluation is described in Section 5. Laboratory experiments are presented and evaluated in Section 6 followed by an error analysis in Section 7. Finally, a summary and conclusions are provided in Section 8.

2. SYSTEM MODEL

In this section, we first describe the concept of DMT-based transmission [30] and the accompanying system and signals used throughout this work. Secondly, the MIMO and the SIMO transmission models are introduced to compactly represent the transmission on a complete cable binder. Any reader familiar with these topics could skip directly to Section 3, where these transmission models are used for deriving the proposed estimator.

2.1. Discrete multitone transmission

Consider the DSL system depicted in Figure 3, which consists of a transmitter and a receiver located in an ADSL2/2+ [12, 13] or VDSL2 [14] modem-pair. The transceivers are connected to a twisted-pair line and employ discrete multitone (DMT) modulation. Without loss of generality, we assume in this section that the same number of subcarriers are used in the downstream and in the upstream direction, that is, the system uses symmetric transmission bandwidths. The DMT-based transceivers use $N/2+1$ frequency domain subcarriers denoted X^k, where k is the subcarrier (subchannel) number, $k = 0, 1, 2, \ldots, N/2$. The carriers are quadrature-amplitude modulated (QAM) and Hermitian extended before being converted to a time-domain DMT symbol (waveform) by an N-point inverse discrete Fourier transform (IDFT). (In practice the IDFT/DFT transform is normally implemented with fast Fourier transform (FFT) techniques.) A cyclic prefix (CP) of L samples is added to the beginning of the time domain symbol before transmission. Hence, by denoting the transmitted frequency domain DMT symbol with the complex vector $\overline{X} = [X^0 \;\; X^1 \;\; \cdots \;\; X^{N-1}]^T$, the cyclic prefix extended time domain symbol can be expressed as (omitting symbol number)

$$\overline{x} = \mathbf{T}\overline{X}, \tag{1}$$

where $\overline{x} = [x_{-L} \;\cdots\; x_0 \;\; x_1 \;\cdots\; x_{N-1}]^T$. The matrix $\mathbf{T}$ denotes the normalized and extended IDFT-matrix defined as

$$\mathbf{T} = \begin{pmatrix} \mathbf{Q_{cp}} \\ \mathbf{Q} \end{pmatrix}. \tag{2}$$

Here, submatrix $\mathbf{Q_{cp}}$ is of size $L \times N$ and contains the L last rows of the $N \times N$ normalized IDFT-matrix $\mathbf{Q}$. A real-valued time domain signal is obtained due to the Hermitian extension of the subcarriers, defined as

$$X^k = \left(X^{k-N/2}\right)^* \quad \text{for } k = N/2+1, \ldots, N-1, \tag{3}$$

where $*$ denotes the complex conjugate. Since X^0 and $X^{N/2}$ (the Nyquist carrier) carry no information, they are here set to zero. The transmission channel in Figure 3 is represented by a stationary impulse response of M samples, denoted by vector $\overline{p} = [p_0 \;\; p_1 \;\cdots\; p_{M-1}]^T$. The disturbance on the line is modeled as additive white Gaussian noise (AWGN) where each noise sample has mean value zero and variance σ^2. Hence, during the symbol transmission, the $(N+L)\times 1$ noise vector $\overline{z}'$ is added to the received signal, where $\overline{z}' \in \mathcal{N}(\overline{0}, \sigma^2 I')$ and I' is the identity matrix of size $(N+L)\times(N+L)$.

The receiver removes the CP of the received time domain signal. By exploiting the cyclic nature of the added prefix, that is, $x_n = x_{N-n}$, for $n = -L, \ldots, -1$, the received signal vector, after removal of CP, can be expressed as

$$\overline{y} = \mathbf{P}\overline{x} + \overline{z} = \mathbf{PT}\overline{X} + \overline{z}, \tag{4}$$

where $\overline{y} = [y_0 \;\; y_1 \;\cdots\; y_{N-1}]^T$, $\overline{z}$ is $N \times 1$ since no CP, and $\mathbf{P}$ is the $N \times (N+L)$ channel convolution matrix. The receiver demodulates the received signal by calculating the discrete Fourier transform (DFT) of the received vector $\overline{y}$. Thus, the received frequency domain vector $\overline{Y} = [Y^0 \;\; Y^1 \;\cdots\; Y^{N-1}]^T$ can, with (4), be expressed as

$$\overline{Y} = \mathbf{R}\overline{y} = \mathbf{RPT}\overline{X} + \overline{Z}, \tag{5}$$

where $\mathbf{R} = \mathbf{Q}^H$ denotes the $N \times N$ normalized DFT matrix, and $\overline{Z}$ is the received frequency domain complex noise vector. Since $\overline{z}$ is uncorrelated, real-valued $\mathcal{N}(\overline{0}, \sigma^2 I)$, where I is the identity matrix of size $N \times N$, it follows that $\overline{Z}$ is complex Gaussian, that is, $\mathcal{CN}(\overline{0}, \sigma^2 I)$, due to the transformation by the normalized DFT-matrix.

It can be shown [30] that if $L > M-1$, matrix $\mathbf{RPT}$ becomes a diagonal matrix $\mathbf{\Lambda}$. Thus, for $L > M-1$, we can rewrite (5) as

$$\overline{Y} = \mathbf{\Lambda}\overline{X} + \overline{Z}, \tag{6}$$

where matrix $\mathbf{\Lambda} = \mathbf{RPT}$ is an $N \times N$ diagonal matrix with the channel frequency response on the main diagonal. In other words, (6) shows that each transmitted subcarrier is independently affected by the transfer function of the channel and no intercarrier interference (ICI) occurs. This property is assumed in this work and can be obtained in practice as described what follows.

For the purpose of estimating the channel, an ADSL/VDSL transmitter repeats the same transmitted DMT symbol. This corresponds to the transmission of the repetitive pseudo-random signal called *Reverb* in the standards [12, 13]. An advantage of using the Reverb signal is the inherent low peak-to-average-power-ratio (PAR) [30]. This type of repetitive transmission can be interpreted as if the cyclic prefix were a multiple of N samples long rather than L, where normally $L \ll N$. Thus, for the case of repeated signals, the channel matrix $\mathbf{RPT}$ becomes diagonalized, and hence, the subchannels become independent. In this work, we will utilize repetitive DMT transmission signals like the Reverb signal, in order to obtain independent subchannels. Hence, the destructive effects of ICI or intersymbol interference (ISI) are of no concern here.

2.2. MIMO transmission

The proposed estimator in Section 3 takes advantage of the MIMO structure of the copper access network, where the underlying MIMO transmission model is described as follows. Figure 1 shows a cable binder with U number of users on each side of the binder, where the twisted-pair lines in the binder are denoted by $u = 1, 2, \ldots, U$. Although the DMT subchannels on a single line are independent under the conditions described in Section 2.1, the electromagnetic coupling between the lines of the binder results in frequency-dependent crosstalk. In fact, the transmitted signal from user u couples (leaks) into all other lines and contribute to the total received crosstalk at the victim receivers. Both near-end crosstalk (NEXT) and far-end crosstalk (FEXT) occur.

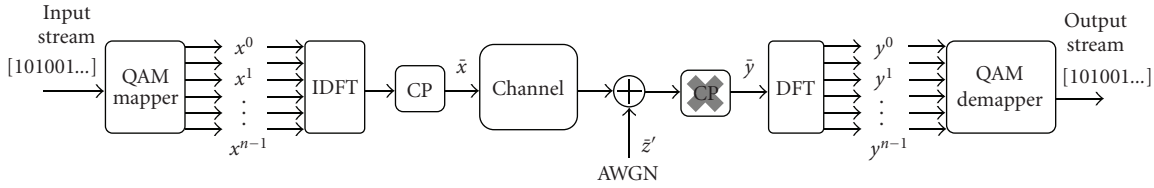

Figure 3: DMT transmission over a twisted-pair channel with additive white Gaussian noise (AWGN). The figure shows the basic transmitter and receiver blocks of the modem-pair.

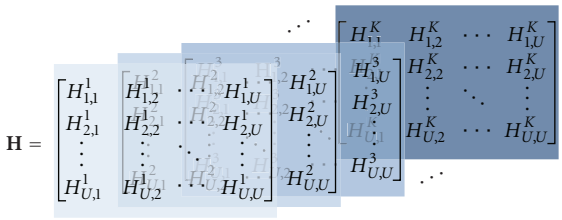

Figure 4: MIMO channel matrix **H** with dimension $U \times U \times K$, where U is the number of lines in the cable binder and K is the number of subchannels in a MIMO group.

In MIMO mathematical modeling for DSL, each user is allocated a user-specific $K_u \leq N/2$ number of subchannels (ignoring DC tone) that depends on the line conditions. However, we will assume in the following description, without loss of generality, that all users are allocated the same number of subchannels, denoted K, where $k = 1, 2, \ldots, K$. In order to model the FEXT channels, we introduce the three-dimensional MIMO FEXT channel matrix **H** of size $U \times U \times K$, which characterizes the transmission through the whole binder from the near-end transmitters to the far-end receivers, that is, the direct channel-paths and the FEXT paths. The matrix channel element $H^k_{n,m}$, as seen in Figure 4, represents the complex-valued FEXT coupling from transmitter m to receiver n for subchannel k. Each complex vector $\overline{H}_{n,m} = [H^1_{n,m}, H^2_{n,m}, \ldots, H^K_{n,m}]^T$ represents the frequency-dependent FEXT transfer function from near-end transmitter m to far-end receiver n. For the case where $m = n$, the vectors $\overline{H}_{1,1}, \overline{H}_{2,2}, \ldots, \overline{H}_{U,U}$ correspond to the direct transfer functions of the individual lines of the binder. Similarly, for $m \neq n$, the off-diagonal elements $\overline{H}_{n,m}$ correspond to the FEXT transfer functions between the lines. In an analogous way to the FEXT, we introduce the three-dimensional MIMO NEXT channel matrix **G** of size $U \times U \times K$, which characterizes the channel from the near-end transmitters to the near-end receivers. The complex vector $\overline{G}_{n,m} = [G^1_{n,m}, G^2_{n,m}, \ldots, G^K_{n,m}]^T$ represents the frequency-dependent NEXT transfer function from near-end transmitter m to near-end receiver n. For $n = m$, the element $G^k_{n,n}$ is by definition zero and of no interest.

In line with Section 2.1, superscript and subscript are used in the following to denote *subchannel*, and *user (line)* number, respectively. Thus, for subchannel k, the transmitted frequency-domain signals on the U lines can be represented by the complex vector $\overline{X}^k = [X^k_1 \; X^k_2 \; \cdots \; X^k_U]^T$. Since the subchannels are assumed independent in this work, we can extend (6) for the MIMO scenario by formulating it as

$$\overline{Y}^k = \mathbf{H}^k \overline{X}^k + \overline{Z}^k, \quad \text{for } k = 1, 2, \ldots, K, \tag{7}$$

where $\mathbf{H}^k$ is the two-dimensional $U \times U$ matrix representing **H** at subchannel k. Here, $\overline{Y}^k = [Y^k_1 \; Y^k_2 \; \cdots \; Y^k_U]^T$ denotes the received (complex) FEXT vector for subchannel k and $\overline{Z}^k = [Z^k_1 \; Z^k_2 \; \cdots \; Z^k_U]^T$ is the (complex) noise vector for subchannel k. In the same way, we model the received NEXT signal as

$$\overline{V}^k = \mathbf{G}^k \overline{X}^k + \overline{W}^k \quad \text{for } k = 1, 2, \ldots, K, \tag{8}$$

where $\overline{V}^k = [V^k_1 \; V^k_2 \; \cdots \; V^k_U]^T$ is the received (complex) NEXT vector in subchannel k, and $\overline{W}^k$ is the (complex) noise vector for subchannel k. From (7), we observe that the received subcarrier Y^k_n, at user n, can be expressed as

$$Y^k_n = H^k_{n,n} X^k_n + \sum_{m=1, m \neq n}^{U} H^k_{n,m} X^k_m + Z^k_n, \quad k = 1, 2, \ldots, K, \quad n = 1, 2, \ldots, U. \tag{9}$$

Hence, the received subcarrier Y^k_n consists of the direct-component $H^k_{n,n} X^k_n$ and the summation of the FEXT contributions from the far-end transmitters plus the additive noise. From (8), it follows that the received subcarrier V^k_n consists of the summation of NEXT contributions from the near-end transmitters plus additive noise. Thus, in order to estimate the cross-talk channels, it is desirable to somehow separate the transmitted signals in (e.g., time-, frequency-, and/or code-domain). In this paper, however, we restrict ourself to the standardized DMT-based DSL systems [12–14], in which case only the time- and frequency-domain can be utilized for signal separation. Since an efficient frequency-separation method would require a co-ordination of the different transmitted signals we instead choose time-separated transmitted signals, as will be described in the following section.

2.3. SIMO transmission

The proposed estimator in Section 3 computes the crosstalk channels of **H** and **G** by exploiting single-input multiple-output (SIMO) transmission instead of MIMO. This corresponds to the case where the transmitted signals are

separated in time-domain, as discussed in the previous section. Figure 2 illustrates the SIMO transmission scenario for a cable binder. By using one transmitter at a time, say m, we simultaneously excite the FEXT and NEXT channels: $\overline{H}_{1,m}, \overline{H}_{2,m}, \ldots, \overline{H}_{U,m}$ and $\overline{G}_{1,m}, \overline{G}_{2,m}, \ldots, \overline{G}_{U,m}$. Thus, with only transmitter m active, it follows from (9) that the received FEXT at far-end receiver n yields

$$\begin{aligned} Y_n^k &= H_{n,m}^k X_m^k + Z_n^k, \\ k &= 1, 2, \ldots, K, \quad n = 1, 2, \ldots, U. \end{aligned} \tag{10}$$

In an analogous way, the received NEXT at the near-end receiver n can be expressed as

$$\begin{aligned} V_n^k &= G_{n,m}^k X_m^k + W_n^k, \\ k &= 1, 2, \ldots, K, \quad n = 1, 2, \ldots, U. \end{aligned} \tag{11}$$

By sequentially activating one transmitter at a time, that is, transmitter $m = 1, 2, \ldots, U$, all channels (elements) of the MIMO matrix $\mathbf{H}$ and $\mathbf{G}$ are excited. This sequential-transmission scheme is exploited by the proposed estimator, as described in the following section.

3. CROSSTALK CHANNEL ESTIMATION

Based on the SIMO transmission model described in the previous section, we derive the optimal NEXT/FEXT estimator in the least-square sense. As the FEXT channels are most important for spectrum management applications, the SIMO FEXT channel estimator is the main focus but the description applies in general also to NEXT channel estimation.

The SIMO system described by (10) and (11) represents a (complex) linear model with additive noise. In contrast to the MIMO case, it is here convenient to consider the transmission from one user at a time and for all K subchannels. In order to simplify the notation, we let transmitter m be active at estimation sequence m. Hence, for estimation sequence m, the SIMO system can be expressed as follows with matrix notation

$$\mathbf{Y}(m) = \mathbf{X}(m)\mathbf{H}(m) + \mathbf{Z}(m), \tag{12}$$

where $\mathbf{Y}(m) = [\overline{Y}_1(m) \;\; \overline{Y}_2(m) \;\; \cdots \;\; \overline{Y}_U(m)]$ is the $K \times U$ matrix containing the received FEXT in all K subchannels and for all U receivers. The $K \times U$ SIMO channel matrix in (12) is represented by $\mathbf{H}(m) = [\overline{H}_{1,m} \;\; \overline{H}_{2,m} \;\; \cdots \;\; \overline{H}_{U,m}]$, which corresponds to column m of $\mathbf{H}$ along the K-dimension. Recall that $\mathbf{H}$ has three dimensions while $\mathbf{H}(m)$ has two. The known $K \times K$ signal matrix from transmitter m yields

$$\mathbf{X}(m) = \begin{pmatrix} X_m^1 & 0 & 0 & 0 \\ 0 & X_m^2 & \ddots & 0 \\ \vdots & \ddots & \ddots & \vdots \\ 0 & \cdots & \cdots & X_m^K \end{pmatrix}, \tag{13}$$

and the added (complex) noise in (12) is denoted by the $K \times U$ matrix $\mathbf{Z}(m) = [\overline{Z}_1(m) \;\; \overline{Z}_2(m) \;\; \cdots \;\; \overline{Z}_U(m)]$. In the following, we assume that the probability density function (PDF) of the noise is unknown, that is, we assume no a priori information about the mean value or the covariance of the noise. Moreover, we assume that the noise is uncorrelated between the receivers since they are (typically) placed at different locations. Subsequently, we choose to apply a least-square (LS) estimator for the SIMO system in (12), which permits an independent processing among the far-end receivers. That is, for estimation sequence m, the received $K \times 1$ FEXT vector at user n yields

$$\overline{Y}_n(m) = \mathbf{X}(m)\overline{H}_{n,m} + \overline{Z}_n(m), \quad \text{for } n = 1, 2, \ldots, U. \tag{14}$$

By minimizing the LS criterion

$$J(\overline{H}_{n,m}) = (\overline{Y}_n(m) - \mathbf{X}(m)\overline{H}_{n,m})^H (\overline{Y}_n(m) - \mathbf{X}(m)\overline{H}_{n,m}), \tag{15}$$

the following LS estimator $\widehat{\overline{H}}_{n,m}(m)$ can be derived [31]:

$$\begin{aligned} \widehat{\overline{H}}_{n,m}(m) &= (\mathbf{X}(m)^H \mathbf{X}(m))^{-1} \mathbf{X}(m)^H \overline{Y}_n(m) \\ &= \mathbf{X}(m)^{-1} \overline{Y}_n(m), \end{aligned} \tag{16}$$

where H denotes the Hermitian transpose, and where the last step of (16) utilizes that $\mathbf{X}(m)$ is a square matrix with full rank. It now follows from (16) that the LS estimator for the SIMO FEXT channel matrix $\mathbf{H}(m)$ can be expressed as

$$\widehat{\mathbf{H}}(m) = \mathbf{X}(m)^{-1}\mathbf{Y}(m). \tag{17}$$

Thus, by sequentially activating transmitter $m = 1, 2, \ldots, U$, the three-dimensional MIMO FEXT channel matrix $\mathbf{H}$ can be estimated via (17). For subchannel k, the LS estimation of the FEXT channel between transmitter m and receiver n can be expressed with (14) and (16) as

$$\begin{aligned} \hat{H}_{n,m}^k = \frac{Y_n^k(m)}{X_m^k} &= H_{n,m}^k + \frac{Z_n^k(m)}{X_m^k}, \\ k &= 1, 2, \ldots, K. \end{aligned} \tag{18}$$

When the (complex-valued) noise sample $Z_n^k(m)$ is considered CAWGN $\mathcal{CN}(0, \sigma^2)$ and uncorrelated with the transmitted signal, it follows from (18) that the estimate $\hat{H}_{n,m}^k$ is unbiased $\mathcal{CN}(H_{n,m}^k, \sigma^2)$ with $|X_m^k|^2 = 1$. By averaging the estimate over M number of DMT symbols, it can be shown that $\hat{H}_{n,m}^k \in \mathcal{CN}(H_{n,m}^k, \sigma^2/M)$. Hence, the variance of the estimate is reduced by a factor of M in this case. In the appendix, we consider the optimum minimum variance unbiased (MVU) estimator for the SIMO system in (12) with CAWGN.

In what follows, we extend the LS estimator in (17) to the case where the phase of the received frequency-domain signal $\mathbf{Y}$ is *not* known. This corresponds to the perspective of an access network operator where only the standardized interfaces of the DMT-based modems [12–14] are accessible. It is, therefore, interesting to consider an estimator based on, for example, the power spectral density (PSD) of standardized transmit and receive signals.

Thus, the intention is to derive an estimator for the square-magnitude of the crosstalk channels, that is, an estimator for the attenuation of the crosstalk channels.

From (12), we note that the received PSD can be expressed as

$$\mathbf{P}_y(m) = \mathbf{P}_x(m)|\mathbf{H}|^2(m) + \mathbf{P}_z(m), \tag{19}$$

where $\mathbf{P}_y(m)$, $\mathbf{P}_x(m)$, and $\mathbf{P}_z(m)$ are the corresponding PSD matrices obtained by taking the absolute-squared value of the elements of $\mathbf{Y}(m)$, $\mathbf{X}(m)$, and $\mathbf{Z}(m)$, respectively. Here, $|\mathbf{H}|^2(m)$ denotes the $K \times U$ FEXT attenuation matrix at estimation sequence m, where matrix element (r, c) of $|\mathbf{H}|^2(m)$ is equal to $|H^r_{c,m}|^2$. Since (19) constitutes a linear model with real-valued additive noise, the LS estimator in (17) provides the PSD-based estimator of $|\mathbf{H}|^2(m)$ by

$$\widehat{|\mathbf{H}|}^2(m) = \mathbf{P}_x(m)^{-1}\mathbf{P}_y(m). \tag{20}$$

Hence, for subchannel k, the PSD-based LS estimate of the square-magnitude of the FEXT channel between transmitter m and receiver n is given by (20) as

$$\widehat{|H^k_{n,m}|}^2 = \frac{|Y^k_n(m)|^2}{|X^k_m|^2} = |H^k_{n,m}|^2 + \frac{|Z^k_n(m)|^2}{|X^k_m|^2}, \quad k = 1, 2, \ldots, K. \tag{21}$$

From (21) we note that the estimate $\widehat{|H^k_{n,m}|}^2$ becomes biased even if the noise can be considered uncorrelated, normal distributed, and with a mean value of zero. To simplify the notation, we select the estimation sequences equidistant in time, that is, we let the estimation sequence number $m = 1, 2, \ldots, U$ also denote the corresponding normalized time instance. This allows the same notation for both estimation sequence-number and measurement time instance. Moreover, we let m_0 denote the time instance between the time instances $m-1$ and m, where $m_0 = m - 1/2$ for $m = 1, 2, \ldots, U$.

In order to mitigate the biased PSD-based estimate of (20), (21), we assume that the noise PSD is stationary over a time span of at least two measurement intervals, which corresponds in practice to a couple of seconds. Before activating transmitter m, the noise PSD is measured with all transmitters silent. The so-obtained (background) noise PSD is denoted $\mathbf{P}_z(m_0)$, where m_0 can be viewed as an initial measurement time instance for sequence m. Transmitter m is thereafter activated and $\mathbf{P}_y(m)$ is measured. Due to the assumed temporarily-stationary condition, we have $\mathbf{P}_z(m) \approx \mathbf{P}_z(m_0)$. An unbiased PSD-based estimate $\widetilde{|\mathbf{H}|}^2(m)$ can be formulated by modifying (20) accordingly:

$$\begin{aligned}\widetilde{|\mathbf{H}|}^2(m) &= \widehat{|\mathbf{H}|}^2(m) - \mathbf{P}_x(m)^{-1}\mathbf{P}_z(m_0) \\ &= |\mathbf{H}|^2(m) - \mathbf{P}_x(m)^{-1}\left(\mathbf{P}_z(m) - \mathbf{P}_z(m_0)\right) \\ &= \mathbf{P}_x(m)^{-1}\left(\mathbf{P}_y(m) - \mathbf{P}_z(m_0)\right).\end{aligned} \tag{22}$$

From the second row of (22), we conclude that the estimate $\widetilde{|\mathbf{H}|}^2(m)$ becomes unbiased if $\mathbf{P}_z(m) = \mathbf{P}_z(m_0)$. The temporary stationarity assumption is reasonable from at least two aspects: in the SIMO case, no other active disturber is present, and the twisted-pair channel is non-time-varying.

We end this section by emphasizing that the square-magnitude of the NEXT channels $\mathbf{G}$ can be estimated with the same estimator as (22) if $\mathbf{P}_y$ and $\mathbf{P}_z$ are interpreted as the received *near-end* signal PSD and *near-end* noise PSD, respectively. In line with Section 2.3, we denote the near-end received $K \times U$ NEXT matrix $\mathbf{P}_v$ and the $K \times U$ near-end noise PSD-matrix $\mathbf{P}_w$. It then follows from (20), (22) that the corresponding PSD-based estimator for the square-magnitude of the NEXT channels yields

$$\widetilde{|\mathbf{G}|}^2(m) = \mathbf{P}_x(m)^{-1}\left(\mathbf{P}_v(m) - \mathbf{P}_w(m_0)\right). \tag{23}$$

4. IMPLEMENTATION

In this section, we outline a practical crosstalk channel estimator that *simultaneously* implements (22) and (23) by using only standardized signals and protocols, supported by off-the-shelf DSL modems compliant with (e.g., [12, 13]). Thus, the focus is on an estimator that can be deployed with equipment already available to the copper access network operator.

The estimator(s) described by (22), (23) utilize the PSD of the near-end and far-end signals. A standardized DSL protocol that contains the measurement of both the far-end and the near-end PSD is the *loop diagnostic* (LD) functionality [12, 13], which is a so-called double-ended line testing (DELT) protocol. The LD procedure is performed synchronously by the near-end and far-end modem for the purpose of line qualification and fault localization. The test requires that the data traffic on the line is temporarily stopped for a couple of seconds while the LD test is performed.

In the following description, we consider the central office (CO) side as the near-end side. The proposed sequential estimation scheme works as illustrated in Figure 5. First in the sequence, the data traffic on all U lines in the binder is stopped. Thereafter, LD is started on all lines simultaneously. The retrieved LD test results contain the measured near-end and far-end PSDs on all U lines. The obtained far-end PSDs is denoted by matrix $\mathbf{P}_z(m_0)$ and the near-end PSDs is denoted by $\mathbf{P}_w(m_0)$. As in Section 3, m_0 denotes the initial measurement time instance at sequence number m, where $m = 1, 2, \ldots, U$. Next, transmitter m is activated and a known test signal is transmitted. The test signal is preferably a pseudo-random repetitive signal which excites the bandwidth of interest with a time period equal to the length of a DMT symbol. Here we assume that the Reverb signal in [12, 13] is used since it is available as a test signal. With this type of signal, the measured subchannels become independent as described in Section 2.1. After activation of the test signal, LD is started on all the other silent $U-1$ lines. The now-obtained far-end and near-end PSDs correspond to $\mathbf{P}_y(m)$ and $\mathbf{P}_v(m)$, respectively. Based on the measured PSDs, (22) and (23) are used to calculate the estimated FEXT and NEXT attenuation matrices $\widetilde{|\mathbf{H}|}^2(m)$ and $\widetilde{|\mathbf{G}|}^2(m)$. The sequential procedure is repeated for $m = 1, 2, \ldots, U$.

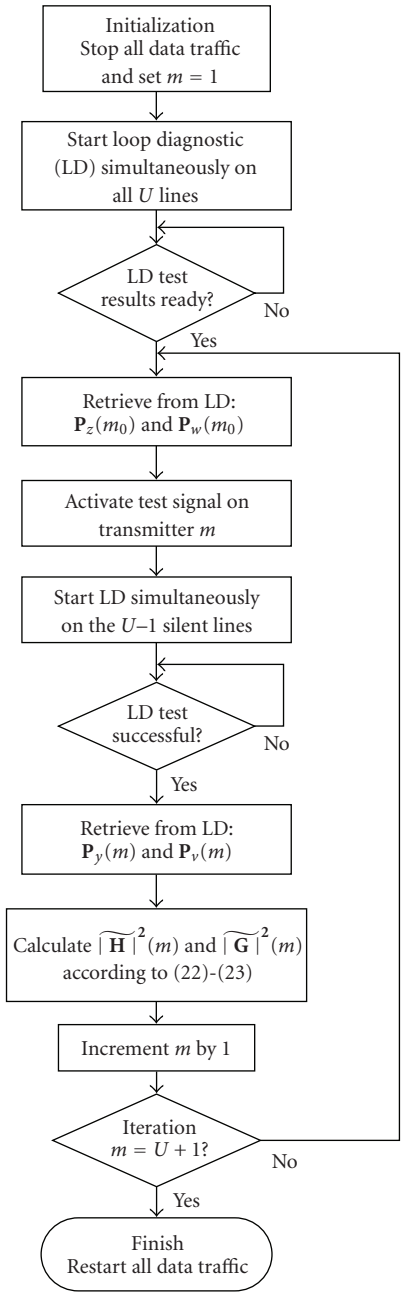

Figure 5: Flow chart of the FEXT and NEXT channel estimator, based on the two-port loop diagnostic (LD) protocol.

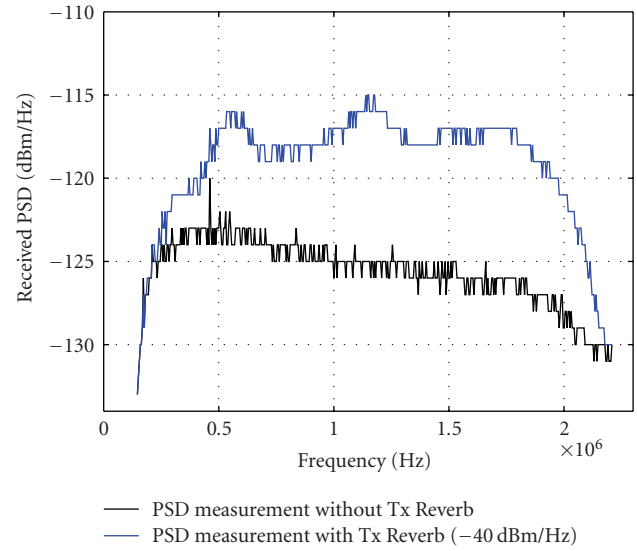

Figure 6: FEXT PSD measurements performed via loop diagnostic (LD) with and without transmitting the Reverb test signal on a neighboring line.

After the last sequence, the U lines are available for data traffic. It should be noted that the crosstalk channels are estimated only for those frequencies that are common for both transmitter m and the receivers in case of different transmit and receive bandwidths.

The LD protocol contains both a silent period, where the *quite-line* PSDs are measured, and a non-silent period with transmission of signals. Hence, it is important that the simultaneously started LD sessions are fairly synchronized on the U lines. Alternatively, one may choose to start LD sequentially on line $1, 2, \ldots, U$ in order to prevent the requirement of synchronization. Furthermore, every time LD is started, the direct transfer function of the channel between the two modems is also estimated by the protocol. Hence, the diagonal elements of the FEXT matrix, which represent the direct channels, are measured at time instance m_0 with high accuracy for both amplitude and phase. It should be emphasized that the described estimation procedure is not restricted to LD since it is based on only PSD measurements. LD is merely a convenient standardized protocol that provides means for executing and retrieving the measurements from a network management level at the CO side. Figure 6 shows an example of the measured FEXT PSDs, when measured by standardized modems, with and without activation of the Reverb test signal on a neighboring line. The figure also shows the quantization effects of the measured PSDs, where each PSD sample from the LD measurement is represented as an integer in dBm/Hz. The impact of this PSD quantization on the estimation performance is analyzed in Section 7.

5. CROSSTALK MODELS

Commonly the NEXT/FEXT channels of a cable binder is represented by the deterministic so-called 99% worst-case model [21] or by any of the more recently published models [24, 32–37]. (The 99% worst-case model is sometime also referred to as the 1% worst-case model. This model has been designed to represent the worst-case of 99% of all the measured crosstalk channels.) These models predict the frequency-dependent square-magnitude of the NEXT/FEXT channels but require a priori information about the line lengths and the line insertion loss or the geometry descriptions of the cable. These properties of the lines, especially the length, may be obtained from a network database or from measurements. However, as can be seen from the

measurements of (e.g., [23]) the FEXT channels between individual lines of the same cable type and length can vary more than 10 dB. Hence, these models are for many crosstalk channels too simple for accurately predicting the crosstalk.

Some of the models [24, 32] are stochastic in the sense that they generate, based on a set of parameters, a random coupling function that represents the NEXT/FEXT channel. The stochastic nature of these kind of models make them less attractive for our needs since a deterministic comparison is desirable. In Section 6, we compare the obtained FEXT channels of the standardized 99% worst-case model with both a reference measurement and the corresponding channels obtained with the proposed estimator in Section 4. In this paper, the 99% worst-case model represents the square-magnitude of the FEXT channels as [21]

$$\left|H_{\text{model}}[f,n,l]\right|^2 = |\text{IL}(f)|^2 \cdot X_F \cdot l \cdot c \cdot f^2, \tag{24}$$

where (i) $|\text{IL}(f)|^2$ denotes the channel insertion loss [30];

(ii) f is the frequency (in Hertz);

(iii) $X_F = 7.74 \times 10^{-21}$ is a coupling constant;

(iv) l is the coupling path length;

(v) c is a distance conversion constant. For l in unit meters $c = 1$, and for l in unit feet, $c = 3.28$ ft/m. For the comparison in Section 6, we employ the model in (24) with the true, (i.e., measured) coupling length l and insertion loss $|\text{IL}(f)|^2$. It should be noticed that the model in (24) disregards the phase information of the channel.

6. LABORATORY EXPERIMENTS

By means of laboratory experiments on real twisted-pair cables, we investigate the performance of the PSD-based FEXT channel estimator, described in Section 4. As NEXT is of less importance for crosstalk mitigation with FDD-based systems, we concentrate the experiments on FEXT channel estimation. The estimation results are compared with the corresponding results obtained with the FEXT model in Section 5 and reference measurements conducted with a network analyzer (NA). The three access network scenarios depicted in Figures 7, 8, and 9 are considered in the comparison. For each scenario, there are two FEXT channels, the *upper* and the *lower* channel, which for scenarios II and III have unequal lengths. The access binders consist of ten 0.40 mm (26 AWG) twisted-pair copper cables of lengths 200 m, 500 m, 700 m, and 1500 m. In Figures 7–9, the transmitter and receiver units are denoted Tx and Rx, respectively. Two laboratory setups are used: one modem-based setup for the FEXT channel estimator and a reference setup. The reference setup is used for the purpose of measuring the "true" square-magnitude of the FEXT channels, which the estimation results are compared with. In both setups the frequency band from 142 kHz to 2.2 MHz is measured with a frequency spacing of 4.3 kHz. This corresponds to the downstream band of ADSL2+. Hence the Tx:s are located at the central office and the cabinet side of the cable binder while the Rx:s are located at the customer-premises side.

The modem-based setup provides an estimate of the square-magnitude of the *total* FEXT channel. That is, the

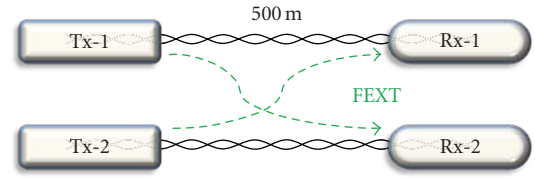

Figure 7: Access network scenario I with two FEXT channels of equal length.

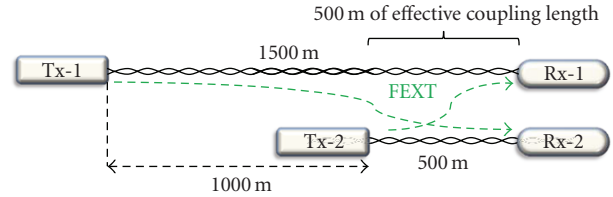

Figure 8: Access network scenario II with two FEXT channels of unequal lengths.

estimate includes the extra attenuation introduced by the low-pass and the high-pass filters of the two DSL transceivers in addition to the physical crosstalk channel. This total channel is the channel of interest for DSM. However, the used FEXT model and the reference measurements are not able to capture the additional attenuation caused by the transceivers. We, therefore, compensate the FEXT model and the reference measurements by including the measured zero-line (i.e., zero-meter) attenuation obtained from LD with the two DSL modems directly connected back-to-back.

6.1. Modem-based setup

The modem-based setup consists of ADSL2+ modems where 100 Ω resistors are used to represent the termination of the nonactive modems of the multipair binder. For all experiments, sequential estimation is employed rather than simultaneous estimation of all SIMO crosstalk channels. The procedure follows the flow chart depicted in Figure 5 and the estimation of the square-magnitude of the FEXT channel is calculated via (22).

6.2. Reference setup

The setup used for the reference measurements is shown in Figure 10. This setup constitutes an established way of measuring the transfer functions of the FEXT channels. The output power of the *HP 4395A Network Analyzer* (NA) is set to 15 dBm (maximum). The *HP 87512A/B Transmission/Reflection Test Set* is used for splitting the signal into two signals: a reference signal and a test signal that is applied to the twisted-pair cable. Hence, the effective power of the inserted test signal is about 7.5 dBm. In order to assure the impedance match, the cable to be measured is connected to the instrument through two baluns (North Hills, wide-band transformer, 0311LB, 10 kHz–60 MHz, 50 Ω UNB,

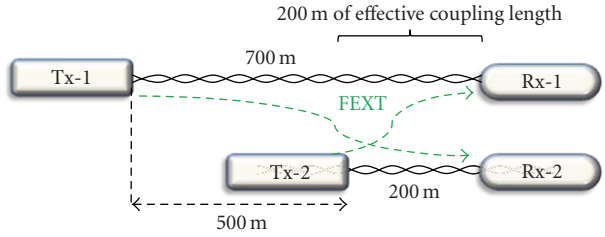

Figure 9: Access network scenario III with two FEXT channels of unequal lengths.

100 Ω BAL). As before, 100 Ω resistors are connected to the unused cable ends.

6.3. Results and comparison

The estimation via (22) can result in negative values for some frequencies due to the variance of the PSDs. Since the attenuation is always positive for passive networks, we consider these negative values as *missing data* rather than zeros, since the latter introduces a too large error. As shown in Figure 6, the measured FEXT PSD is quantized by the modem to integer values in units of dBm/Hz, according to LD protocol. From repeated measurements on the same crosstalk channel, it can be concluded that the obtained FEXT PSDs varies with time in integer steps for a given frequency. The PSD variation between the maximum and the minimum value for a given frequency is typically 1–3 dBm/Hz with our setup. At the measurement, band-edges, a variation up to 4–6 dBm/Hz can be observed for some crosstalk channels. From the measurements it can also be concluded that the level of variation is independent of the magnitude of the received PSD. The impact of the time-variation on the FEXT channel estimate is analyzed further in Section 7 and provides some insight to the estimation errors.

For each access network scenario in Figures 7, 8, and 9, the square-magnitude of the two FEXT channels are estimated and measured with the modem-based setup and the reference setup, respectively. Figures 11, 12, 13, 14, 15, and 16 show the estimation results of the two FEXT channels in access network scenario I, II, and III, respectively. The corresponding worst-case FEXT model in (24) is also plotted in Figures 11–16 for comparison, given the true line length and insertion loss. For all scenarios, it can be observed, as expected, that the difference between the NA measurement and the FEXT model is larger than the corresponding difference between the NA measurement and the proposed FEXT estimator. This is true for all used frequencies. The transceiver-filter compensation of the NA measurement and the FEXT model can be seen as increasing (more negative) attenuation at the band edges, that is, high-pass and low-pass filtering. Except for a small estimation offset for scenario I at certain frequencies, the shape of the estimation curve follows the curvature of the NA measurement quite well. This ability of the estimator is especially important for DSM algorithms that exploit the peaks and the valleys of the FEXT channels in the search for the optimum transmission PSDs.

It can be noted that the estimation results contain a few number of missing data points for all scenarios at the lower frequency-band edge. This is due to the high-pass filter of the transceiver(s) which causes the received signal, measured with active test-signal, to drown in the background noise. This can also be seen for the typical FEXT channel in Figure 6 where the received signal PSDs are overlapping at frequencies below 250 kHz. Hence, at these frequencies, no estimation via (22) is possible due to power limitation of maximum −40 dBm/Hz regulated by the DSL standards [12, 13]. It is, however, possible to use interpolation and/or extrapolation of the estimation results in order to recapture the missing data.

Although the variance of the estimates is different for the considered FEXT channels, as seen in Figures 11–16, we can state that the proposed FEXT estimator has a mean deviation less than 3 dB relative to the NA measurements for most frequencies. In fact, preprocessing of the estimation results with, for example, a moving average filter reduces the variance of the estimates and gives a mean deviation typically less than 2 dB. The change in the variance of the estimates is analyzed further in the following section.

7. ERROR ANALYSIS

The internal (thermal) noise of the transceivers, and extrinsic noise, cause the obtained PSDs to vary (slightly) with time. The impact of this PSD variation, combined with the measurement quantization, is analyzed in this section. In what follows, we focus on the FEXT estimator in (22), but the analysis is also valid for the NEXT estimator in (23).

The estimator(s) described by (22) and (23) rely(relies) on the assumption of stationary background noise PSD during the two consecutive measurements at time instance m_0 and m, for example, it is assumed that $\mathbf{P}_z(m) \approx \mathbf{P}_z(m_0)$ for the FEXT case, and $\mathbf{P}_w(m) \approx \mathbf{P}_w(m_0)$ for the NEXT case. As before, we use the same notation for estimation sequence number and measurement time instance. Without loss of generality, we simplify the notations by considering only one subcarrier (frequency) and a certain FEXT channel, for example, scalar quantities are used in this section.

With an implementation of the estimator according to Section 4, the PSD is measured as integer values in units of dBm/Hz. (The unit dBm/Hz is a power-measure that expresses the transmit/receive power relative to 1 mW, in logarithmic scale.) Let us denote the true received PSD at estimation sequence m by $P_{\mathrm{dBm\,Hz}}(m)$, where the frequency dependence is omitted. Before calculating the FEXT channel estimate, the obtained PSDs are converted to linear scale by

$$P(m) = 10^{(P_{\mathrm{dBm\,Hz}}(m,f)-30)/10}B, \tag{25}$$

where B is the measurement bandwidth in Hz. After this conversion, the FEXT channel estimate in (22) yields

$$\widetilde{|H|}^2(m) = \frac{P_y(m) - P_z(m_0)}{P_x(m)}, \tag{26}$$

where all quantities are scalar-values in linear scale. Furthermore, $P_z(m_0)$ is the PSD-measurement of the background

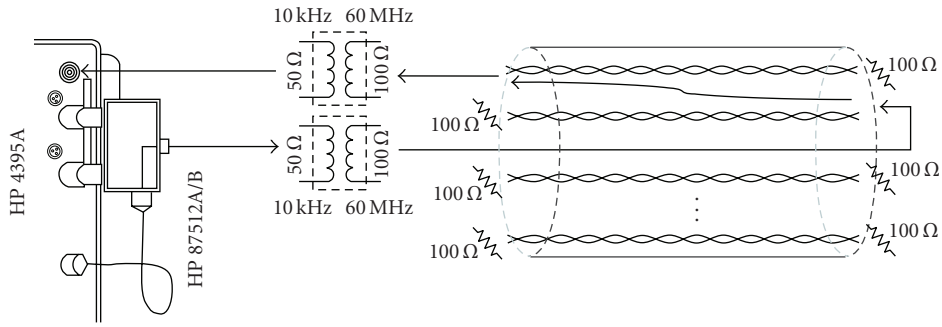

Figure 10: Reference setup for measuring the FEXT transfer functions with a Network Analyzer (NA).

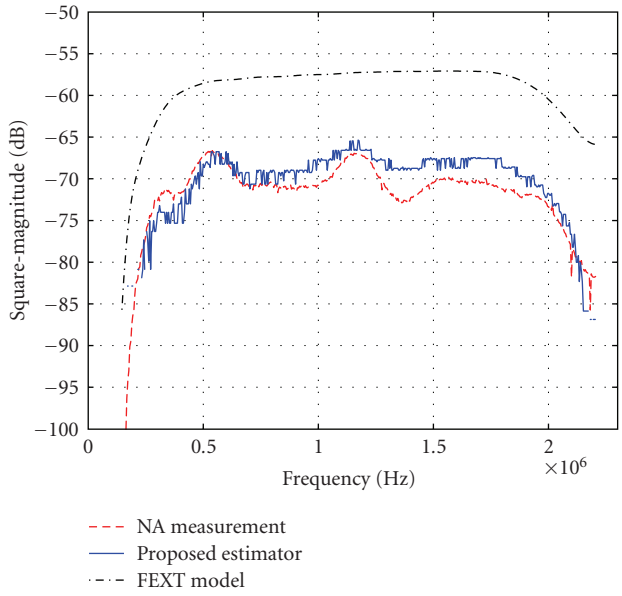

Figure 11: Square-magnitude of the upper FEXT channel in access network scenario I obtained with the NA, the FEXT model, and the proposed estimator.

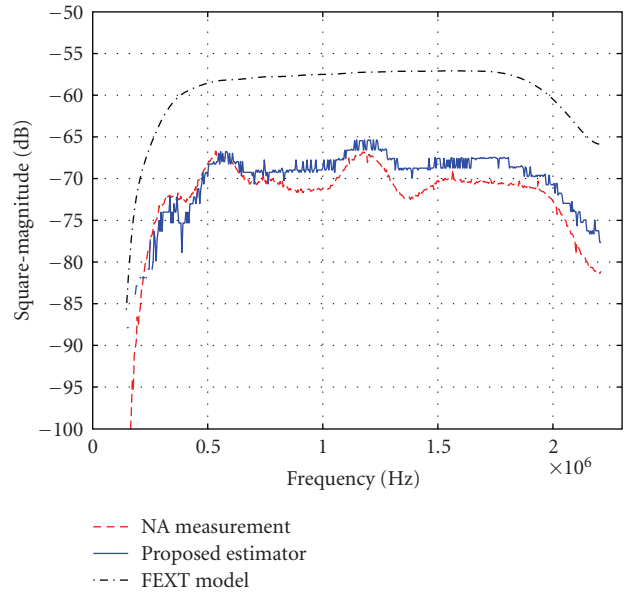

Figure 12: Square-magnitude of the lower FEXT channel in access network scenario I obtained with the NA, the FEXT model, and the proposed estimator.

noise at time instance m_0, and $P_y(m)$ is the corresponding PSD measurement with an active Reverb test-signal on a neighboring line. Here, $P_x(m)$ is the (known) PSD of the test signal. The measurement quantization due to the LD protocol [12, 13], in combination with the additive noise, causes the obtained PSD values (in logarithmic scale) to fluctuate in integer steps around the mean value. The PSD measurements can, therefore, be described as

$$\hat{P}_{\mathrm{dBm\,Hz}}(m) = P_{\mathrm{dBm\,Hz}}(m) + \Delta_{\mathrm{dBm\,Hz}}(m), \tag{27}$$

where $P_{\mathrm{dBm\,Hz}}(m)$ is the nonquantized PSD and $\Delta_{\mathrm{dBm\,Hz}}(m)$ is the quantized measurement error, modeled as a discrete integer-valued random variable with uniform distribution, that is, $\Delta_{\mathrm{dBm\,Hz}}(m) \in \{-\delta, -\delta+1, \ldots, 0, \ldots, \delta\}$dBm/Hz. From Section 6.3, we know that δ is typically in the order of 1–3 dBm/Hz, and independent of the magnitude of the received PSD. Consequently, for the case where the received FEXT is (significantly) larger than the background noise, that is, $P_y(m) \gg P_z(m_0)$, the measurement error of $P_z(m_0)$ has little or no impact on the FEXT channel estimate compared to the error of $P_y(m)$. With this assumption, the measurement error at time instance m_0 can be neglected, and the FEXT channel estimate of (26) yields, with (25) and (27),

$$\widetilde{|H|}^2(m) = \frac{P_y(m)\Delta(m) - P_z(m_0)}{P_x(m)}, \tag{28}$$

where $\Delta(m)$ is the corresponding measurement error in linear scale. Expressed in decibel, the FEXT channel estimate is $\widetilde{|H|}^2_{\mathrm{dB}}(m) = 10\log_{10}\widetilde{|H|}^2(m)$. Subsequently, the estimation error defined as the ratio of (26) and (28), in logarithmic scale, can be formulated as

$$\begin{aligned}\mathrm{Error}_{\mathrm{dB}}(m) &= 10\,\log_{10}\frac{P_y(m) - P_z(m_0)}{P_y(m)\Delta(m) - P_z(m_0)} \\ &= 10\log_{10}\frac{1 - P_z(m_0)/P_y(m)}{\Delta(m) - P_z(m_0)/P_y(m)}.\end{aligned} \tag{29}$$

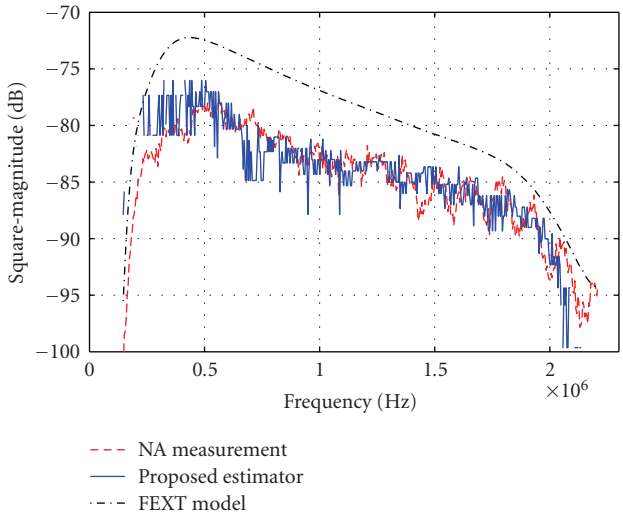

Figure 13: Square-magnitude of the upper (longer) FEXT channel for access network scenario II obtained with the NA, the FEXT model, and the proposed Estimator.

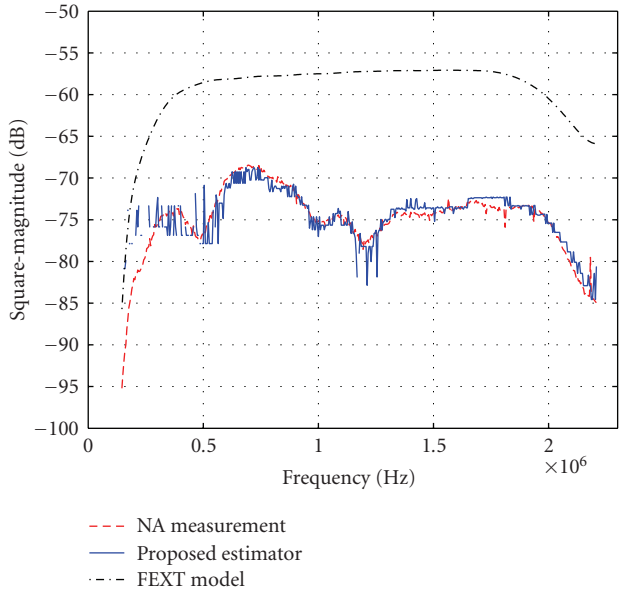

Figure 14: Square-magnitude of the lower (shorter) FEXT channel for access network scenario II obtained with the NA, the FEXT model, and the proposed estimator.

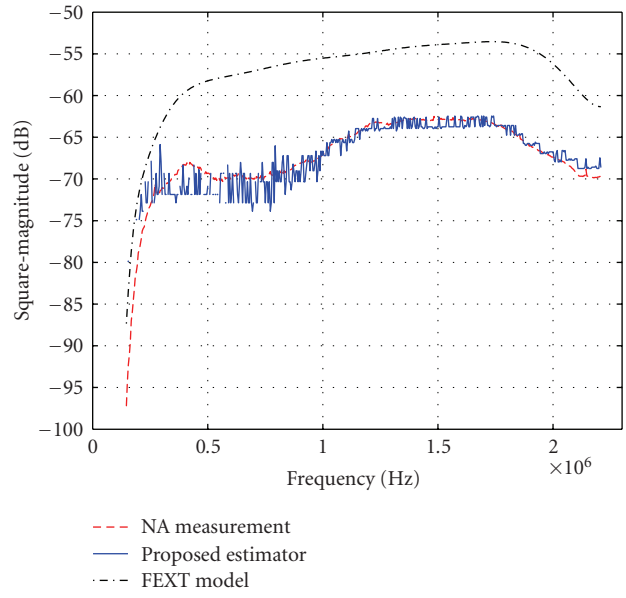

Figure 15: Square-magnitude of the upper (longer) FEXT channel for access network scenario III obtained with the NA, the FEXT model, and the proposed estimator.

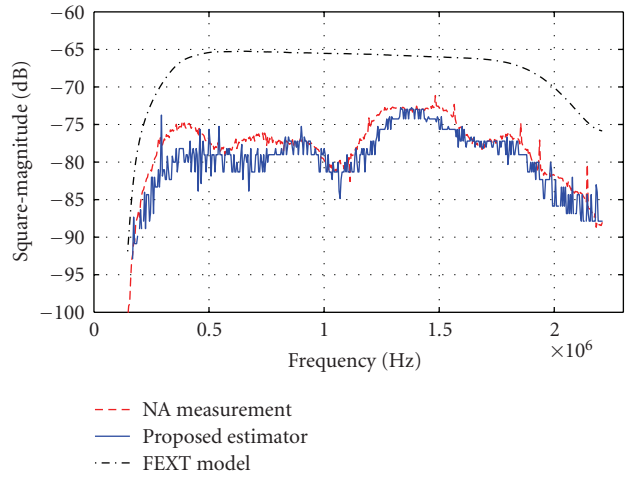

Figure 16: Square-magnitude of the lower (shorter) FEXT channel for access network scenario III obtained with the NA, the FEXT model and the proposed estimator.

However, (29) shows that the measurement error affects the FEXT channel estimate in a nonlinear way. Of particular interest is the fact that the estimation error is a function of the ratio (in linear scale) between the two consecutive measurements at time instance m_0 and m. However, with the assumption $P_y(m) \gg P_z(m_0)$, the estimation error becomes $\text{Error}_{\text{dB}}(m) \approx 10\log_{10}(1/\Delta(m))$, which has a linear dependence on the measurement error in logarithmic scale. Note that error-free measurements correspond to $\Delta_{\text{dBm Hz}}(m) \to -\infty$ which with (25) gives $\Delta(m) \to 1$.

Figure 17 shows the FEXT channel estimation error in (29) as a function of the measurement error $\Delta(m)$ and the background noise $P_z(m_0)$. The received FEXT PSD $P_y(m)$ with active test signal is here fixed to -100 dBm/Hz, which corresponds to a transmitted test signal $P_x(m)$ of -40 dBm/Hz and an FEXT channel attenuation of 60 dB. Figure 17 suggests that the estimation error increases more than linearly when the level of the background noise $P_z(m_0)$ approaches $P_y(m)$. When the difference between $P_y(m)$ and $P_z(m_0)$ becomes larger than 5 dBm/Hz, the estimation error is approximately linear with the measurement error. For the case $P_z(m_0) \geq P_y(m)$, no estimation is possible which is depicted in Figure 17 as missing data.

The changes in the estimation variance, seen in, for example, Figure 15, as a larger variance for frequencies below 1 MHz, can be explained with the aforementioned

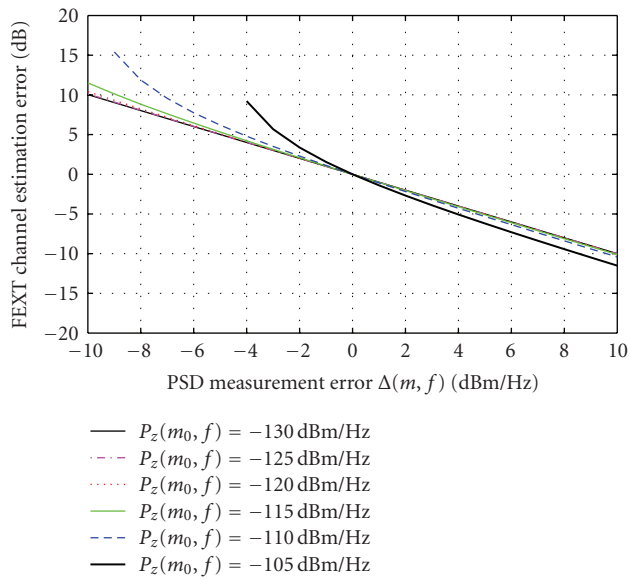

FIGURE 17: The FEXT channel estimation error in (29) as a function of the PSD measurement error $\Delta(m)$ and the received background noise $P_z(m_0)$. The received FEXT PSD $P_y(m)$ from the neighboring line is here fixed to -100 dBm/Hz.

analysis. In fact, a closer inspection of the measured PSDs for the FEXT channel in Figure 15 reveals that $P_y(m) \approx P_z(m_0)$ for frequencies below 1 MHz while $P_y(m) \gg P_z(m_0)$ for frequencies above 1 MHz. Thus, in line with (29), the measurement error becomes amplified in the FEXT channel estimate for frequencies below 1 MHz in Figure 15. The same increase in estimation variance can be observed for the other scenarios where $P_y(m) \approx P_z(m_0)$.

8. SUMMARY AND CONCLUSIONS

DSM crosstalk mitigation techniques for the copper access network requires information about the *square magnitude* (attenuation) of the crosstalk channels. The paper addresses this issue by proposing an estimator that is capable to simultaneously obtain the square-magnitude of the FEXT and NEXT channels. The proposed estimator is derived from least-square estimation of a linear SIMO system with AWGN. The additional requirement of only utilizing PSD-signals for the LS estimator results in a biased estimate. However, by assuming stationary conditions during the short estimation period, the estimator is made unbiased by subtracting the measured background PSD at the receiver.

The proposed estimator requires no hardware or software changes of the used DSL modems and utilizes only measurements available via the existing DSL standards. An implementation based on the standardized *loop diagnostic* (LD) functionality was described and evaluated by laboratory experiments on three access network scenarios, built up with twisted-pair copper cables. A comparison with reference measurements indicate that the mean deviation of the estimator is less than 3 dB for most frequencies. In particular, the ability of the estimator to follow the curvature of the FEXT channels was demonstrated, which is an important property for DSM that the compared FEXT channel model is missing.

APPENDIX

Here, we consider the optimum minimum variance-unbiased (MVU) estimator for the SIMO linear model of (12) with complex AWGN. The noise is assumed uncorrelated between different receivers, and hence, independent between receivers for the Gaussian case. We may, therefore, study (12) from a single-receiver perspective. Thus, with only transmitter m active at estimation sequence m, the (complex) FEXT at receiver n can be expressed as

$$\overline{Y}_n(m) = \mathbf{X}(m)\overline{H}_{n,m} + \overline{Z}_n(m), \quad \text{for } n = 1, 2, \ldots, U, \tag{A.1}$$

where $\overline{Y}_n(m)$ is the $K \times 1$ received FEXT vector from transmitter m, $\overline{H}_{n,m}$ is the FEXT channel from transmitter m to receiver n, and $\mathbf{X}(m)$ denotes the $K \times K$ transmit matrix, all defined in Section 3. Here, $\overline{Z}_n(m) \in \mathcal{CN}(\overline{0}, \mathbf{C})$, where the mean-value vector is zero and the $K \times K$ positive definite covariance matrix is denoted by $\mathbf{C}$. In order to simplify the notation, we drop the subscript and the sequence number in the following analysis. Under the assumed conditions, the PDF of the received vector is given by

$$f_Y(\overline{H}) = \frac{1}{\pi^K \det \mathbf{C}} \exp\left(-\frac{1}{2}(\overline{Y} - \mathbf{X}\overline{H})^H \mathbf{C}^{-1}(\overline{Y} - \mathbf{X}\overline{H})\right). \tag{A.2}$$

The maximum likelihood estimator (MLE) maximizes $\ln f_Y(\overline{H})$ which is equivalent to minimize the exponent of (A.2). Hence, the MLE minimizes

$$J = (\overline{Y} - \mathbf{X}\overline{H})^H \mathbf{C}^{-1}(\overline{Y} - \mathbf{X}\overline{H}), \tag{A.3}$$

where H denotes the Hermitian transpose. Since $\mathbf{C}^{-1}$ is a positive definite matrix and J is a quadratic function of the elements of $\overline{H}$, the global minimum is obtained by expanding (A.3) and completing the square, that is

$$\begin{aligned} J = {} & (\overline{H} - (\mathbf{X}^H\mathbf{C}^{-1}\mathbf{X})^{-1}\mathbf{X}^H\mathbf{C}^{-1}\overline{Y})^H \mathbf{X}^H\mathbf{C}^{-1}\mathbf{X} \\ & \cdot (\overline{H} - (\mathbf{X}^H\mathbf{C}^{-1}\mathbf{X})^{-1}\mathbf{X}^H\mathbf{C}^{-1}\overline{Y}) + \overline{Y}^H\mathbf{C}^{-1}\overline{Y} \\ & - \overline{Y}^H\mathbf{C}^{-1}\mathbf{X}(\mathbf{X}^H\mathbf{C}^{-1}\mathbf{X})^{-1}\mathbf{X}^H\mathbf{C}^{-1}\overline{Y}. \end{aligned} \tag{A.4}$$

The quadratic term in (A.4) is always nonnegative and thus J is minimized for

$$\overline{H}_{\text{MLE}} = (\mathbf{X}^H\mathbf{C}^{-1}\mathbf{X})^{-1}\mathbf{X}^H\mathbf{C}^{-1}\overline{Y}, \tag{A.5}$$

where the index MLE stands for maximum likelihood estimator. It can further be shown [31] that the PDF of the MLE is complex normal distributed as

$$\overline{H}_{\text{MLE}} \in \mathcal{CN}(\overline{H}, (\mathbf{X}^H\mathbf{C}^{-1}\mathbf{X})^{-1}). \tag{A.6}$$

For a general linear model with complex AWGN, as (A.1) represents, it can be shown [31] that the MLE is an MVU

estimator as well as an efficient estimator in that it attains the Cramer-Rao lower bound. However, the estimator in (A.5) requires the inverted noise covariance matrix $\mathbf{C}^{-1}$ which is not available from a network operator's point of view, where only standardized signals can be retrieved. In case the noise is uncorrelated, $\mathbf{C}$ becomes a diagonal matrix and the MLE in (A.5) is reduced to $\mathbf{X}^{-1}\overline{Y}$, provided that $\mathbf{X}$ has full rank. This case corresponds to the least-square estimator in (16).

ACKNOWLEDGMENTS

This work was partially supported by the Research and Development Center, Ericsson Telecommunications S.A., Brazil. Some of the authors acknowledge financial support from the Swedish Agency for Innovation Systems, VINNOVA, through the Eureka-Celtic BANITS project.

REFERENCES

[1] K. J. Kerpez, "DSL spectrum management standard," *IEEE Communications Magazine*, vol. 40, no. 11, pp. 116–123, 2002.

[2] K. J. Kerpez, D. L. Waring, S. Galli, J. Dixon, and P. H. Madon, "Advanced DSL management," *IEEE Communications Magazine*, vol. 41, no. 9, pp. 116–123, 2003.

[3] J. Verlinden, T. Bostoen, and G. Ysebaert, "Dynamic spectrum management for digital subscriber lines—edition 2," Technology White Paper—Alcatel, 2005.

[4] NIPP-NAI-2007-038 R3, "Draft dynamic spectrum management technical report for second default ballot," 2007.

[5] R. Cendrillon and M. Moonen, "Iterative spectrum balancing for digital subscriber lines," in *Proceedings of IEEE International Conference on Communications (ICC '05)*, vol. 3, pp. 1937–1941, Seoul, Korea, May 2005.

[6] R. Cendrillon, W. Yu, M. Moonen, J. Verlinden, and T. Bostoen, "Optimal multiuser spectrum balancing for digital subscriber lines," *IEEE Transactions on Communications*, vol. 54, no. 5, pp. 922–933, 2006.

[7] J. Papandriopoulos and J. S. Evans, "Low-complexity distributed algorithms for spectrum balancing in multi-user DSL networks," in *Proceedings of IEEE International Conference on Communications (ICC '06)*, vol. 7, pp. 3270–3275, Istanbul, Turkey, July 2006.

[8] R. Cendrillon, J. Huang, M. Chiang, and M. Moonen, "Autonomous spectrum balancing for digital subscriber lines," *IEEE Transactions on Signal Processing*, vol. 55, no. 8, pp. 4241–4257, 2007.

[9] D. Statovci, T. Nordström, and R. Nilsson, "Dynamic spectrum management for standardized VDSL," in *Proceedings of IEEE International Conference on Acoustics, Speech and Signal Processing (ICASSP '07)*, vol. 3, pp. 73–76, Honolulu, Hawaii, USA, April 2007.

[10] J. M. Cioffi, S. Jagannathan, W. Lee, et al., "Greener copper with dynamic spectrum management," AccessNets, Las Vegas, Nev, USA, 2008.

[11] S. Jagannathan, C. S. Hwang, and J. M. Cioffi, "Margin optimization in digital subscriber lines employing level-2 dynamic spectrum management," in *Proceedings of IEEE International Conference on Communications (ICC '08)*, pp. 435–440, Beijing, China, May 2008.

[12] ITU-T Standard G.992.3, "Asymmetric digital subscriber line transceivers 2 (ADSL2)," January 2005.

[13] ITU-T Standard G.992.5, "Asymmetric digital subscriber line (ADSL) transceivers—extended bandwidth ADSL2 (ADSL2plus)," January 2005.

[14] ITU-T Standard G.993.2, "Very high speed digital subscriber line transceivers 2 (VDSL2)," February 2006.

[15] T. Bostoen, P. Boets, M. Zekri, L. Van Biesen, T. Pollet, and D. Rabijns, "Estimation of the transfer function of a subscriber loop by means of a one-port scattering parameter measurement at the central office," *IEEE Journal on Selected Areas in Communications*, vol. 20, no. 5, pp. 936–948, 2002.

[16] S. Galli and D. L. Waring, "Loop makeup identification via single ended testing: beyond mere loop qualification," *IEEE Journal on Selected Areas in Communications*, vol. 20, no. 5, pp. 923–935, 2002.

[17] T. Vermeiren, T. Bostoen, P. Boets, X. Ochoa Chehab, and F. Louage, "Subscriber loop topology classification by means of time-domain reflectometry," in *Proceedings of IEEE International Conference on Communications (ICC '03)*, vol. 3, pp. 1998–2002, Anchorage, Alaska, USA, May 2003.

[18] P. Boets, L. Van Biesen, T. Bostoen, and D. Gardan, "Single-ended line testing—a white box approach," in *Proceedings of the 4th IASTED International Multi-Conference on Wireless and Optical Communications*, pp. 393–398, Banff, Canada, July 2004.

[19] S. Galli and K. J. Kerpez, "Single-ended loop make-up identification—part I: a method of analyzing TDR measurements," *IEEE Transactions on Instrumentation and Measurement*, vol. 55, no. 2, pp. 528–537, 2006.

[20] K. J. Kerpez and S. Galli, "Single-ended loop-makeup identification—part II: improved algorithms and performance results," *IEEE Transactions on Instrumentation and Measurement*, vol. 55, no. 2, pp. 538–549, 2006.

[21] American National Standard for Telecommunications, "Spectrum Management for Loop Transmission Systems, T1.417-2003, (issue 2)," 2003.

[22] ITU-T Standard G.996.1, "Test procedures for digital subscriber line (DSL) transceivers," February 2001.

[23] N. Fonseca, D. Neves, A. C. Gomes, et al., "Evaluation of DSM performance with mixed DSL services and measured crosstalk channels," in *Proceedings of the 25th Simpósio Brasileiro de Telecomunicações (SBrT '07)*, Recife, Brazil, September 2007.

[24] M. Sorbara, P. Duvaut, F. Shmulyian, S. Singh, and A. Mahadevan, "Construction of a DSL-MIMO channel model for evaluation of FEXT cancellation systems in VDSL2," in *Proceedings of IEEE Sarnoff Symposium (SARNOFF '07)*, pp. 1–6, Princeton, NJ, USA, April 2007.

[25] C. Zeng, C. Aldana, A. A. Salvekar, and J. M. Cioffi, "Crosstalk identification in xDSL systems," *IEEE Journal on Selected Areas in Communications*, vol. 19, no. 8, pp. 1488–1496, 2001.

[26] S. Galli, C. Valenti, and K. J. Kerpez, "A frequency-domain approach to crosstalk identification in xDSL systems," *IEEE Journal on Selected Areas in Communications*, vol. 19, no. 8, pp. 1497–1506, 2001.

[27] N. Papandreou and T. Antonakopoulos, "Far-end crosstalk identification method based on channel training sequences," *IEEE Transactions on Instrumentation and Measurement*, vol. 54, no. 6, pp. 2204–2212, 2005.

[28] Y. Shi, F. Ding, and T. Chen, "Multirate crosstalk identification in xDSL systems," *IEEE Transactions on Communications*, vol. 54, no. 10, pp. 1878–1886, 2006.

[29] ITU-T Study Group 15, "G.vector: Draft Recommendation," December 2008.

[30] T. Starr, J. M. Cioffi, and P. J. Silverman, *Understanding Digital Subscriber Line Technology*, Prentice-Hall, Englewood Cliffs, NJ, USA, 1999.

[31] S. M. Kay, *Fundamentals of Statistical Signal Processing: Estimation Theory*, Prentice Hall Signal Processing Series, Prentice-Hall, Englewood Cliffs, NJ, USA, 1993.

[32] C. Valenti, "NEXT and FEXT models for twisted-pair North American loop plant," *IEEE Journal on Selected Areas in Communications*, vol. 20, no. 5, pp. 893–900, 2002.

[33] S. Galli and K. J. Kerpez, "Methods of summing crosstalk from mixed sources—part I: theoretical analysis," *IEEE Transactions on Communications*, vol. 50, no. 3, pp. 453–461, 2002.

[34] K. J. Kerpez and S. Galli, "Methods of summing crosstalk from mixed sources—part II: performance results," *IEEE Transactions on Communications*, vol. 50, no. 4, pp. 600–607, 2002.

[35] E. Karipidis, N. Sidiropoulos, A. Leshem, L. Youming, R. Tarafi, and M. Ouzzif, "Crosstalk models for short VDSL2 lines from measured 30 MHz data," *EURASIP Journal on Applied Signal Processing*, vol. 2006, Article ID 85859, 9 pages, 2006.

[36] B. Lee, J. M. Cioffi, S. Jagannathan, et al., "Binder MIMO channels," *IEEE Transactions on Communications*, vol. 55, no. 8, pp. 1617–1628, 2007.

[37] ITU-T Study Group 15—Contribution 30, "Status of ATIS NIPP-NAI Technical Report on MIMO Crosstalk Channel Model," November 2008.